



## The di-lepton physics program at STAR

Lijuan Ruan for the STAR Collaboration

Physics Department, Brookhaven National Laboratory, Upton NY 11973

---

### Abstract

The recent results on di-electron production in  $p+p$  and Au+Au collisions at  $\sqrt{s_{NN}} = 200$  GeV are presented. The cocktail simulations of di-electrons from light and heavy flavor hadron decays are reported and compared with data. The perspectives for di-lepton measurements in lower energy Au+Au collisions and with future detector upgrades are discussed.

**Keywords:** di-electron continuum, cocktail simulation, low-mass enhancement, QGP thermal radiation,  $\mu - e$  correlation

---

### 1. Introduction

Ultra-relativistic heavy ion collisions provide a unique environment to study the properties of strongly interacting matter at high temperature and high energy density [1]. One of the crucial probes of this strongly interacting matter are di-lepton measurements in the low and intermediate mass region. Di-leptons are not affected by the strong interaction once produced, therefore they can probe the whole evolution of the collision.

In the low invariant mass range of produced lepton pairs ( $M_{ll} < 1.1$  GeV/ $c^2$ ), we can study vector meson in-medium properties through their di-lepton decays, where modifications of mass and width of the spectral functions observed may relate to the possibility of chiral symmetry restoration [2, 3]. At the SPS, the low mass di-lepton enhancement in the CERES  $e^+e^-$  data [4] and in the NA60  $\mu^+\mu^-$  data [5] requires substantial medium effects on the  $\rho$ -meson spectral function. The precise NA60 measurement of the low mass enhancement provides a decisive discrimination between a dropping-mass scenario [6] and a massively broadened spectral function [7]. The latter one was found to be able to consistently describe the data.

The di-lepton spectra in the intermediate mass range ( $1.1 < M_{ll} < 3.0$  GeV/ $c^2$ ) are directly related to thermal radiation of the Quark-Gluon Plasma (QGP) [2, 3]. However, contributions from other sources have to be measured experimentally. Such contributions include background pairs from correlated open heavy flavor decays, which produce a pair of electrons or muons from the semileptonic decay of a pair of open charm or bottom hadrons ( $c\bar{c} \rightarrow l^+l^-X$  or  $b\bar{b} \rightarrow l^+l^-X$ ).

Anisotropic flow, an anisotropy in the particle production relative to the reaction plane, leads to correlations among particles [8]. The elliptic flow  $v_2$  is the second harmonic of the azimuthal distribution of particles with respect to the reaction plane.  $v_2$  has been measured for direct photons and found to be substantial in the transverse momentum range  $1 < p_T < 4$  GeV/ $c$  in central 0-20% Au+Au collisions at  $\sqrt{s_{NN}} = 200$  GeV [9]. In the same  $p_T$  region, PHENIX measured direct photon yields and found an excess of direct photon yield in 0-20% Au+Au over  $p+p$ , exponential

---

Email address: [ruanlj@rcf.rhic.bnl.gov](mailto:ruanlj@rcf.rhic.bnl.gov), [ruan@bnl.gov](mailto:ruan@bnl.gov) (Lijuan Ruan for the STAR Collaboration)

in  $p_T$  [10]. Model calculations [11] for QGP thermal photons in this kinematic region significantly under-predict the observed  $v_2$  while if a significant contribution from the hadronic sources at later stages is added, the excess of the spectra and the observed  $v_2$  at  $1 < p_T < 4$  GeV/c are described reasonably well [12]. It has been proposed that di-lepton  $v_2$  measurements will provide another independent way to study medium properties since di-leptons provide two independent kinematic parameters: mass and  $p_T$ . Specifically,  $v_2$  as a function of  $p_T$  in different mass regions will enable us to probe the properties of medium from a hadron-gas dominated to a QGP dominated scenario [13].

At STAR, the newly installed Time-of-Flight detector (TOF) offers large acceptance and high efficiency [14]. The TOF, combined with measurements of ionization energy loss (dE/dx) from the Time Projection Chamber (TPC) [15, 16, 17], enables electron identification with high purity for  $0.2 < p_T < 3$  GeV/c [18, 19, 20]. In this article we present the di-electron mass spectra in  $p + p$  and Au+Au collisions at  $\sqrt{s_{NN}} = 200$  GeV. The elliptic flow  $v_2$  measurements are also reported in 200 GeV Au+Au collisions. Future capabilities for di-lepton measurements at STAR in lower energy Au+Au collisions and with detector upgrades are discussed.

## 2. Recent results on di-electron production

We utilize 107 million, 270 million and 150 million events for  $p + p$ , minimum-bias (0-80%) Au+Au, and central (0-10%) Au+Au di-electron analyses, respectively. The  $p + p$  events were taken in 2009 when 72% of the full TOF system was installed and operational, while the Au+Au events were taken in 2010 with full TOF system coverage. By applying velocity and dE/dx cuts on tracks with  $p_T > 0.2$  GeV/c, we can achieve the purity for the electron candidates of about 99% in  $p + p$  collisions and 97% in minimum-bias Au+Au collisions.

The di-electron signals may come from light and heavy flavor hadron decays. They include  $\pi^0$ ,  $\eta$ , and  $\eta'$  Dalitz decays:  $\pi^0 \rightarrow \gamma e^+ e^-$ ,  $\eta \rightarrow \gamma e^+ e^-$ , and  $\eta' \rightarrow \gamma e^+ e^-$ ; vector meson decays:  $\omega \rightarrow \pi^0 e^+ e^-$ ,  $\omega \rightarrow e^+ e^-$ ,  $\rho^0 \rightarrow e^+ e^-$ ,  $\phi \rightarrow \eta e^+ e^-$ ,  $\phi \rightarrow e^+ e^-$ , and  $J/\psi \rightarrow e^+ e^-$ ; heavy-flavor hadron semi-leptonic decays:  $c\bar{c} \rightarrow e^+ e^- X$  and  $b\bar{b} \rightarrow e^+ e^- X$ ; and Drell-Yan contributions. In Au+Au collisions, we look for additional vector meson in-medium modifications in the low mass region and possible QGP thermal radiations in the intermediate mass range.

The  $e^+$  and  $e^-$  pairs from the same events are combined to reconstruct the invariant mass distributions ( $M_{ee}$ ) marked as unlike-sign distributions. The unlike-sign distributions contain both signal and background. The background contains random combinatorial pairs and correlated pairs. The electron candidates are required to be in the range of  $|\eta| < 1$  and  $p_T > 0.2$  GeV/c while  $e^+ e^-$  pairs are required to be in the rapidity range of  $|y_{ee}| < 1$ . Two methods are used for background estimation, based on same-event like-sign and mixed-event unlike-sign techniques. In the like-sign technique, electron pairs with the same charge sign are combined from the same events. In the mixed-event technique, unlike-sign pairs are formed from different events. In  $p + p$  collisions, we subtract the like-sign background at  $M_{ee} < 0.4$  GeV/c<sup>2</sup> and mixed-event background in the higher-mass region. In Au+Au collisions, we subtract the like-sign background at  $M_{ee} < 0.7$  GeV/c<sup>2</sup> and mixed-event background in the higher-mass region. The detailed analysis procedures including background subtraction and systematic uncertainty evaluations are published for  $p + p$  results in [21] and presented for Au+Au results in [22, 23].

After the efficiency correction, the di-electron mass spectra within the STAR acceptance are shown in Fig. 1 for  $p + p$ , minimum-bias Au+Au and central Au+Au collisions at  $\sqrt{s_{NN}} = 200$  GeV. The di-electron mass spectra are not corrected for momentum resolution and radiation energy loss effect. The ratios of data to cocktail simulations are shown in the lower panels. In  $p + p$  collisions, the cocktail simulation, which includes the expected components from light and heavy flavor meson decays, is consistent with the measured di-electron continuum within uncertainties [21]. The  $\chi^2/NDF$  between data and cocktail simulation are 21/26 for  $M_{ee} > 0.1$  GeV/c<sup>2</sup> and 8/7 for  $1.1 < M_{ee} < 3.0$  GeV/c<sup>2</sup>. In the mass region  $0.2 < M_{ee} < 0.8$  GeV/c<sup>2</sup>, the cocktail simulation is systematically higher than the measured di-electron continuum. However, they are also consistent within uncertainties. We find that better agreement between the cocktail simulation and data can be achieved by applying an additional scale factor (56%) to the  $\eta$  Dalitz decay contribution. Further details on the decay and cocktail simulations are published in [21]. We also find that the  $c\bar{c} \rightarrow e^+ e^- X$  contribution is dominant in the intermediate mass region in  $p + p$  collisions. In Au+Au collisions, the  $\rho^0$  contribution is not included and the  $c\bar{c} \rightarrow e^+ e^- X$  contribution is from PYTHIA simulation [24] with the total charm cross section 0.96 mb, scaled by the number of underlying binary nucleon-nucleon collisions. In the low mass region  $0.15 < M_{ee} < 0.75$  GeV/c<sup>2</sup>, the possible enhancement factors, the ratios of the data to the cocktail simulations, are  $1.53 \pm 0.07 \pm 0.41$  and  $1.72 \pm 0.10 \pm 0.50$  in minimum-bias and central collisions, respectively. This suggests for possible vector meson in-medium modification in this low mass region. The models [25, 26, 27], which describe

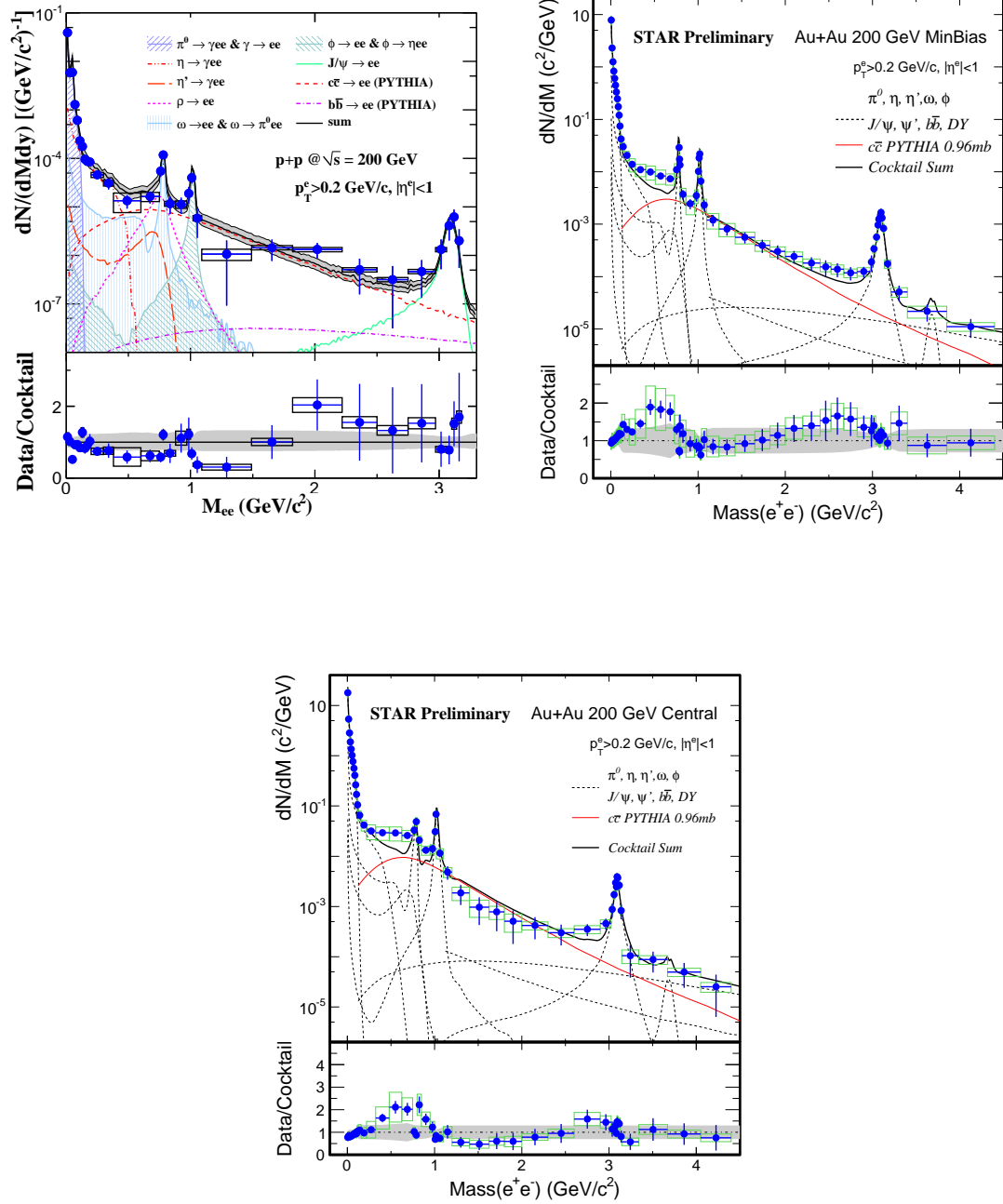


Figure 1: (Color online) The comparison for di-electron continuum between data and simulation after efficiency correction within the STAR acceptance in  $p + p$  (upper-left panel), minimum-bias (upper-right panel) Au+Au and central (bottom panel) Au+Au collisions at  $\sqrt{s_{NN}} = 200$  GeV. The di-electron continuum from simulations with different source contributions are also shown. The Drell-Yan contribution in  $p+p$  collisions is not shown but included in the total cocktail contribution. The bars and boxes (bands) represent statistical and systematic uncertainties, respectively. The bands on the bottom panels illustrate the systematic uncertainties on the cocktail simulation.

the SPS di-lepton data but fail to consistently describe the PHENIX low- $p_T$  and low-mass enhancement [28], can describe our data reasonably well. The comparison between data and models can be found in [23, 26, 27]. Differential measurements as a function of  $p_T$  and centrality are on-going.

In the low mass region, we obtain the invariant yields of  $\omega$  and  $\phi$  through di-electronic decays at mid-rapidity ( $|y| < 1$ ) in  $p + p$  and Au+Au collisions at  $\sqrt{s_{NN}} = 200$  GeV, shown in Fig. 2. In  $p + p$  collisions, our  $\omega$  yields from di-electron decays [21] are consistent with previous results [29] and a prediction from a Tsallis fit, which fits spectra of other particles and high  $p_T$  ( $p_T > 2$  GeV/c)  $\omega$  yields [30, 31]. In Au+Au collisions, we fit light hadrons simultaneously using Tsallis function [30], obtain the freeze-out parameters, predict the shape of the  $\omega$  invariant yield versus  $p_T$ , and find it describes our measurement  $\omega \rightarrow e^+e^-$  [32] reasonably well. This indicates that the  $\omega \rightarrow e^+e^-$  flow pattern is similar to that of light hadrons in Au+Au collisions. Shown in Fig. 2 (right panel) is the comparison of the invariant yields of  $\phi$  through its  $e^+e^-$  [33] and  $K^+K^-$  [34] decays. Within statistical and systematic uncertainties, the  $\phi$  invariant yields measured through  $e^+e^-$  and  $K^+K^-$  decays are consistent.

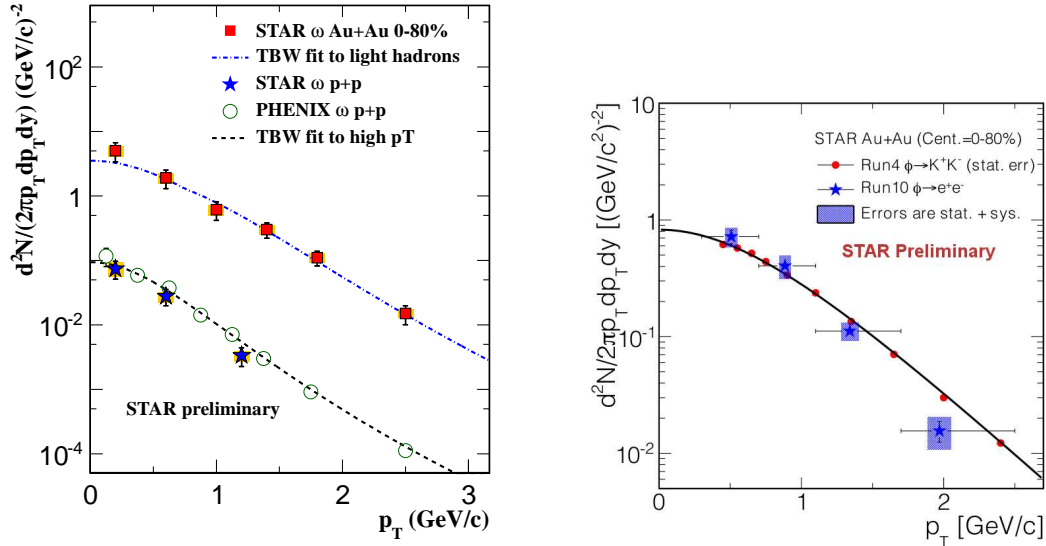


Figure 2: (Color online) (left panel) The  $\omega$  invariant yield measured through di-electronic decay as a function of  $p_T$  at mid-rapidity ( $|y| < 1$ ) in  $p + p$  and minimum-bias Au+Au collisions at  $\sqrt{s_{NN}} = 200$  GeV. The open circles represent PHENIX published results [29]. The dashed line represents the yields of  $\omega$  from Tsallis function (TBW) fit to other particles and high  $p_T$   $\omega$  yields in  $p + p$  collisions at  $\sqrt{s} = 200$  GeV. The dot-dashed line represents the yields of  $\omega$  from Tsallis fit to other particles in Au+Au collisions at  $\sqrt{s_{NN}} = 200$  GeV. The bars and boxes represent statistical and systematic uncertainties, respectively. (right panel) The  $\phi$  invariant yield measured through di-electronic and  $K^+K^-$  decays as a function of  $p_T$  at mid-rapidity ( $|y| < 1$ ) in minimum-bias Au+Au collisions at  $\sqrt{s_{NN}} = 200$  GeV. The curve represents an exponential fit to the  $\phi \rightarrow K^+K^-$  data points. The bars represent statistical errors. The boxes represent the quadrature sum of statistical and systematic uncertainties.

The di-lepton  $v_2$  measurements provide another independent way to study the medium properties. We use event-plane method to obtain the di-electron  $v_2$ . The event-plane is reconstructed using the tracks from the TPC. The details of the method are in Refs. [8, 35]. We report the  $v_2$  of di-electron signals in Fig. 3 (upper-left panel) as a function of  $M_{ee}$  in minimum-bias Au+Au collisions at  $\sqrt{s_{NN}} = 200$  GeV. The differential  $v_2$  of di-electron pairs in the mass regions of  $M_{ee} < 0.14$   $\text{GeV}/c^2$  and  $0.14 < M_{ee} < 0.30$   $\text{GeV}/c^2$  are shown respectively in the upper-right and bottom panels of Fig. 3 as a function of  $p_T$  in minimum-bias Au+Au collisions at  $\sqrt{s_{NN}} = 200$  GeV. Also shown are the charged [36] and neutral pion [37]  $v_2$ . The dominant sources to di-electrons at  $M_{ee} < 0.14$   $\text{GeV}/c^2$  and  $0.14 < M_{ee} < 0.30$   $\text{GeV}/c^2$  are

$\pi^0$  Dalitz decay and  $\eta$  Dalitz decay, respectively. We parameterize the pion  $v_2$  from low to high  $p_T$  [36, 37], perform the Dalitz decay simulation, and obtain the expected di-electron  $v_2$  from  $\pi^0$  Dalitz decay shown by the solid curve. The simulated  $v_2$  is consistent with the measured di-electron  $v_2$  at  $M_{ee} < 0.14$  GeV/ $c^2$ . The consistency between the expectations and measurements demonstrates the credibility of our method to obtain the di-electron  $v_2$ . We repeat the same exercise in the  $\eta$  mass region. We assume that  $\eta$  has the same  $v_2$  as  $K_S^0$  [35] since the  $\eta$  mass is close to that of  $K_S^0$ . The simulated  $v_2$  of di-electrons from  $\eta$  Dalitz decay, shown as a solid curve, is consistent with the measured di-electron  $v_2$  at  $0.14 < M_{ee} < 0.30$  GeV/ $c^2$ . The current precision of our  $v_2$  data does not allow to further study a possible deviation from the solid curve due to the other contributions in this mass region.

Figure 4 (left panel) shows the di-electron  $v_2$  as a function of  $p_T$  in minimum-bias Au+Au collisions at  $\sqrt{s_{NN}} = 200$  GeV for  $0.5 < M_{ee} < 0.7$  GeV/ $c^2$  in which charm correlation and in-medium  $\rho$  contribution might be dominant. Right panel of Fig. 4 shows the di-electron  $v_2$  as a function of  $p_T$  in the mass ranges of  $0.76 < M_{ee} < 0.8$  GeV/ $c^2$  and  $0.98 < M_{ee} < 1.06$  GeV/ $c^2$  in minimum-bias Au+Au collisions at  $\sqrt{s_{NN}} = 200$  GeV. The di-electrons  $v_2$  for  $0.98 < M_{ee} < 1.06$  GeV/ $c^2$  is consistent with the measured  $v_2$  of  $\phi$  meson through the  $K^+K^-$  decay [38].

### 3. Future perspectives

A factor of two more Au+Au data at  $\sqrt{s_{NN}} = 200$  GeV, taken in 2011, will significantly improve the measurements of mass spectra and elliptic flow. The possible low mass enhancement factors for  $0.15 < M_{ee} < 0.75$  GeV/ $c^2$  are significantly lower than those measured by PHENIX in minimum-bias and central collisions [23]. The  $p_T$  dependence measurements in the future will allow more differential comparisons between STAR and PHENIX. In addition, di-electron  $v_2$  as a function of  $p_T$  in the intermediate mass region  $1.1 < M_{ee} < 2.9$  GeV/ $c^2$  will be obtained.

In 2010 and 2011, STAR has taken a few hundred million minimum-bias events in Au+Au collisions at  $\sqrt{s_{NN}} = 19.6, 27, 39,$  and  $62.4$  GeV with full TOF azimuthal coverage and low conversion material budget, which will enable us to systematically study the energy dependence of the following physics topics: 1) di-electron enhancement in the low mass region [39, 40]; 2) in-medium modifications of vector meson decays; 3) virtual photons [10]; 4)  $c\bar{c}$  medium modifications; and 5) possible QGP thermal radiation in the intermediate mass region. Specifically, the energy value of 19.6 GeV is comparable to the center of mass energy for the CERES and NA60 measurements. The di-electron results in Au+Au collisions at  $\sqrt{s_{NN}} = 19.6$  GeV will enable another consistency check between STAR measurements and previous SPS results.

With the current data sets, it will be difficult to measure charm correlation contribution or QGP thermal radiation in the intermediate mass region since they are coupled to each other and one is the other's background for the physics case. So far at RHIC, there is no clear answer about thermal radiation in the intermediate mass region. The future detector upgrade with the Heavy Flavor Tracker at STAR, to be completed in 2014, will provide precise charm cross section measurements [41]. This will help to understand heavy quark dynamics in the medium and constrain model inputs to calculate di-leptons from heavy flavor correlations. However the measurements of  $c\bar{c}$  correlations will still be challenging if not impossible. An independent approach is proposed with the Muon Telescope Detector upgrade (MTD) [42]. The  $\mu - e$  correlations measure the contribution from heavy flavor correlations to the di-electron or di-muon continuum. This will make it possible to access the thermal radiation in the intermediate mass region.

The MTD construction, to be completed in 2014, has started. In 2012, 10% of the MTD was installed at STAR and worked nicely with smooth data taking. This will enable a first proof-of-principle for  $\mu - e$  measurement. In 2013, 43% of MTD will be installed and we request three-week Au+Au run at 200 GeV for the  $\mu - e$  measurement. Figure 5 shows the precision projections for  $\mu - e$  invariant mass distribution and azimuthal angular correlation from charm correlation contribution from simulation in Au+Au collisions at  $\sqrt{s_{NN}} = 200$  GeV for Run 2013. If the  $\mu - e$  correlation is not modified in Au+Au collisions, the precision projection is indicated by the circle shown in Fig. 5 (left panel) for 280 million central events. Also shown for the comparison is the case that  $c$  and  $\bar{c}$  is de-correlated illustrated by the black line. In addition, with full azimuthal coverage of the TPC, TOF, and Barrel Electro-magnetic Calorimeter (BEMC), we will be able to measure  $\mu - e$  azimuthal angular correlation. Figure 5 (right panel) illustrates the precision projection for  $\mu - e$  azimuthal angular correlation from PYTHIA simulation when we sample  $2 nb^{-1}$  Au+Au luminosity with a coincidence trigger of single muon hit and BEMC energy deposition above a certain threshold. The projection is done under the assumption that the correlation is the same as in PYTHIA.

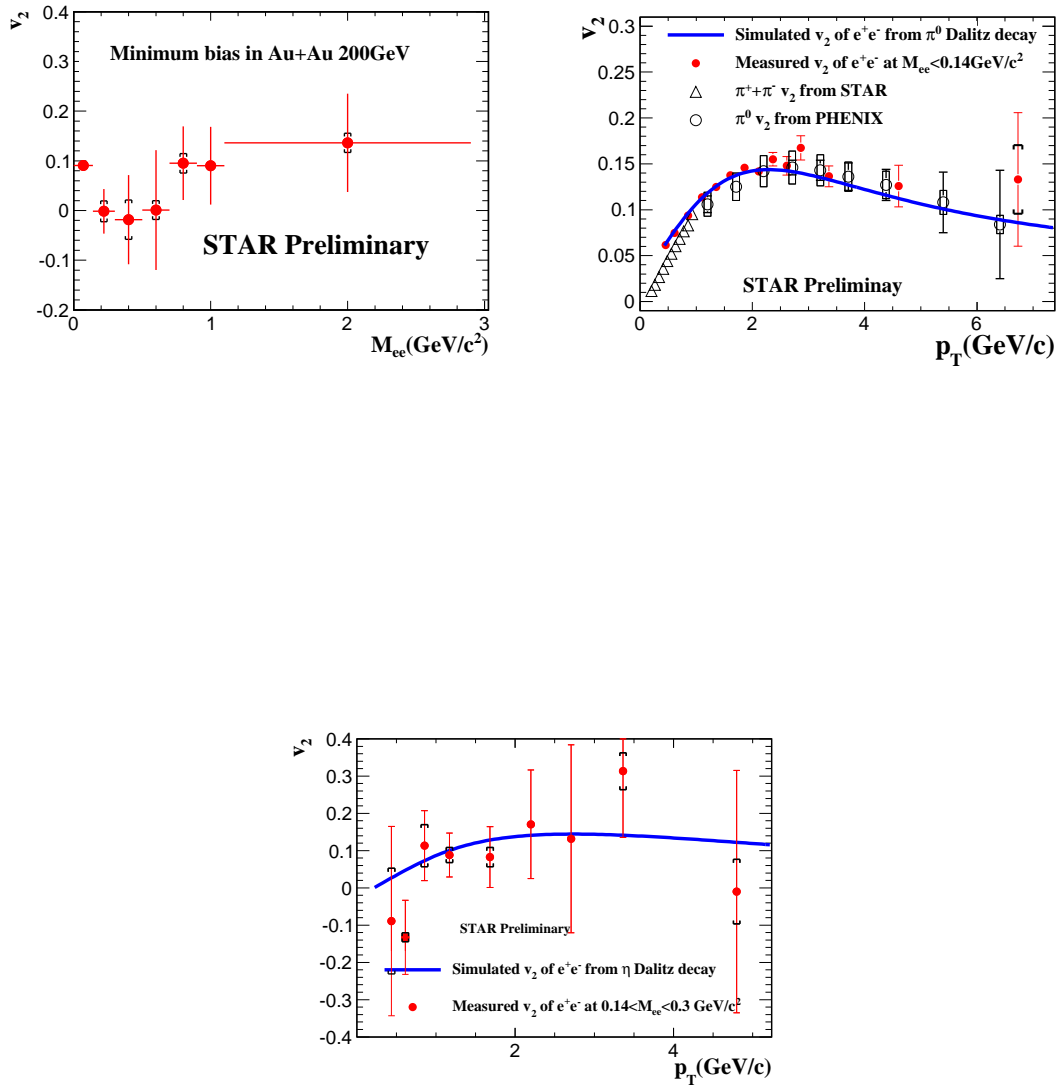


Figure 3: (Color online) (upper-left panel) The di-electron  $v_2$  as a function of  $M_{ee}$  in minimum-bias Au+Au collisions at  $\sqrt{s_{NN}} = 200$  GeV. (upper-right panel) The  $v_2$  of di-electron at  $M_{ee} < 0.14$  GeV/c<sup>2</sup> (solid symbols) as a function of  $p_T$  in minimum-bias Au+Au collisions at  $\sqrt{s_{NN}} = 200$  GeV. Also shown are the charged and neutral pion  $v_2$  and the expected  $v_2$  (solid curve) of di-electrons from  $\pi^0$  Dalitz decay. (bottom panel) The  $v_2$  of di-electron at  $0.14 < M_{ee} < 0.30$  GeV/c<sup>2</sup> as a function of  $p_T$  in minimum-bias Au+Au collisions at  $\sqrt{s_{NN}} = 200$  GeV. Also shown is the expected  $v_2$  (solid curve) of di-electrons from  $\eta$  Dalitz decay. The bars and boxes represent statistical and part of systematic uncertainties, respectively.

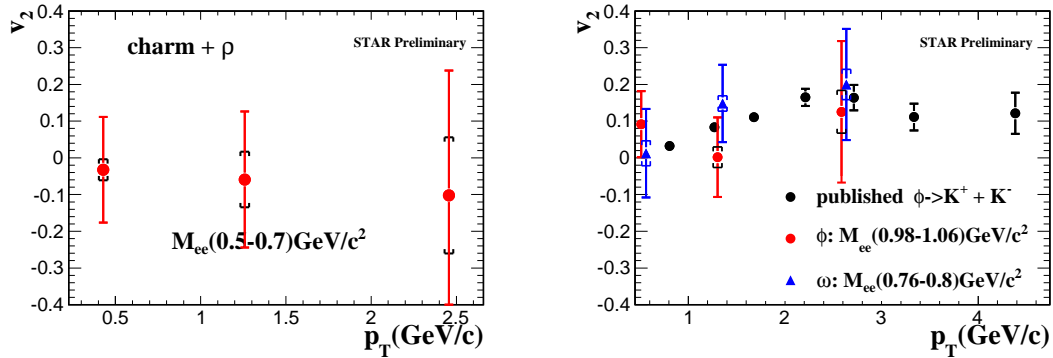


Figure 4: (Color online) The di-electron  $v_2$  as a function of  $p_T$  in minimum-bias Au+Au collisions at  $\sqrt{s_{NN}} = 200$  GeV for  $0.5 < M_{ee} < 0.7$   $\text{GeV}/c^2$  (left),  $0.76 < M_{ee} < 0.8$   $\text{GeV}/c^2$ , and  $0.98 < M_{ee} < 1.06$   $\text{GeV}/c^2$  (right). Also shown is the measured  $v_2$  of  $\phi$  meson through the  $K^+K^-$  decay. The bars and boxes represent statistical and part of systematic uncertainties, respectively.

#### 4. Summary

In summary, the di-electron mass spectra are measured in 200 GeV  $p + p$  and Au+Au collisions at STAR. The cocktail simulations are consistent with the data in 200 GeV  $p + p$  collisions. In Au+Au collisions, we observe a possible enhancement by comparison between data and cocktail simulation in the low mass region  $0.15 < M_{ee} < 0.75$   $\text{GeV}/c^2$ . The first elliptic flow measurements of di-electrons are presented in 200 GeV minimum-bias Au+Au collisions. The  $v_2$  of di-electrons at  $M_{ee} < 0.14$   $\text{GeV}/c^2$  and  $0.14 < M_{ee} < 0.30$   $\text{GeV}/c^2$  are in agreement with the expectations from previous measurements. In the future, more precise differential measurements will be obtained for di-electron spectra and  $v_2$  at 200 GeV. The data taken at lower energies will allow to systematically study the energy dependence of low-mass enhancement. The precise charmed hadron measurements from future detector upgrade with the Heavy Flavor Tracker will help to constrain model inputs to calculate di-leptons from heavy flavor correlations. The  $\mu - e$  correlations with the Muon Telescope Detector upgrade will measure the contribution from heavy flavor correlations to the di-electron or di-muon continuum. This will make it possible to access the thermal radiation in the intermediate mass region.

#### References

- [1] J. Adams *et al.*, Nucl. Phys. A **757**, 102 (2005).
- [2] R. Rapp and J. Wambach, Adv. Nucl. Phys. **25**, 1 (2000).
- [3] G. David, R. Rapp and Z. Xu, Phys. Rept. **462**, 176 (2008).
- [4] G. Agakichiev *et al.*, Eur. Phys. J. C **41**, 475 (2005).
- [5] R. Arnaldi *et al.*, Phys. Rev. Lett. **96**, 162302 (2006).
- [6] G.E. Brown and M. Rho, Phys. Rep. **269**, 333 (1996).

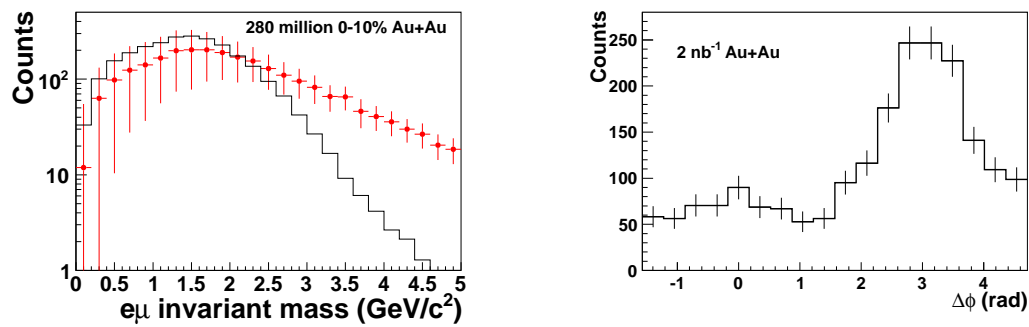


Figure 5: (Color online) (left panel) The precision projection for  $\mu - e$  invariant mass distribution from charm correlation contribution from simulation in Au+Au collisions at  $\sqrt{s_{NN}} = 200$  GeV for Run 2013. The circles represent the case that the  $\mu - e$  correlation is not modified in Au+Au collisions for 280 million central events. The black line represents the case that  $c$  and  $\bar{c}$  is de-correlated. (right panel) The precision projection for  $\mu - e$  azimuthal angular correlation from charm correlation contribution from PYTHIA simulation for Run 2013 when we sample  $2 \text{ nb}^{-1}$  Au+Au luminosity with a coincidence trigger of single muon hit and BEMC energy deposition above a certain threshold. The projection is done under the assumption that the correlation is the same as in PYTHIA.

- [7] R. Rapp and J. Wambach, Eur. Phys. J. A **6**, 415 (1999); H. van Hees and R. Rapp, Nucl. Phys. A **806**, 339 (2008); T. Renk and J. Ruppert, Phys. Rev. C **77**, 024907 (2008).
- [8] A.M. Poskanzer and S.A. Voloshin, Phys. Rev. C **58**, 1671 (1998).
- [9] A. Adare *et al.*, arXiv: 1105.4126.
- [10] A. Adare *et al.*, Phys. Rev. Lett. **104**, 132301 (2010).
- [11] R. Chatterjee and D.K. Srivastava, Phys. Rev. C **79**, 021901(R) (2009).
- [12] H. van Hees, C. Gale, and R. Rapp, Phys. Rev. C **84**, 054906 (2011).
- [13] R. Chatterjee *et al.*, Phys. Rev. C **75**, 054909 (2007).
- [14] B. Bonner *et al.*, Nucl. Instr. Meth. A **508**, 181 (2003); M. Shao *et al.*, Nucl. Instr. Meth. A **492**, 344 (2002); J. Wu *et al.*, Nucl. Instr. Meth. A **538**, 243 (2005).
- [15] M. Anderson *et al.*, Nucl. Instr. Meth. A **499**, 659 (2003).
- [16] H. Bichsel, Nucl. Instr. Meth. A **562**, 154 (2006).
- [17] Y. Xu *et al.*, Nucl. Instr. Meth. A **614**, 28 (2010).
- [18] M. Shao *et al.*, Nucl. Instr. Meth. A **558**, 419 (2006).
- [19] J. Adams *et al.*, Phys. Lett. B **616**, 8 (2005).
- [20] J. Adams *et al.*, Phys. Rev. Lett. **94**, 062301 (2005).
- [21] L. Adamczyk *et al.*, Phys. Rev. C **86**, 024906 (2012); L. Ruan *et al.*, Nucl. Phys. A **855**, 269 (2011).
- [22] J. Zhao *et al.*, J. Phys. G **38**, 124134 (2011).
- [23] J. Zhao *et al.*, Hard Probes 2012 proceedings, arXiv: 1207.6987.
- [24] T. Sjöstrand *et al.*, Comput. Phys. Commun. **135**, 238 (2001).
- [25] R. Rapp, J. Wambach, and H. van Hees, arXiv:0901.3289.
- [26] O. Linnyk *et al.*, Phys. Rev. C **85**, 024910 (2012).
- [27] H. Xu *et al.*, Phys. Rev. C **85**, 024906 (2012).
- [28] A. Adare *et al.*, Phys. Rev. C **81**, 034911 (2010).
- [29] A. Adare *et al.*, Phys. Rev. D **83**, 052004 (2011).



- [30] Z. Tang *et al.*, Phys. Rev. C **79**, 051901 (2009); M. Shao *et al.*, J. Phys. G **37**, 085104 (2010).
- [31] S.S. Adler *et al.*, Phys. Rev. C **75**, 051902 (2007).
- [32] B. Huang *et al.*, A. Phys. Pol. B Supp. **5**, 471 (2012).
- [33] M. Wada *et al.*, A. Phys. Pol. B Supp. **5**, 249 (2012).
- [34] B.I. Abelev *et al.*, Phys. Rev. C **79**, 064903 (2009).
- [35] B.I. Abelev *et al.*, Phys. Rev. C **77**, 054901 (2008).
- [36] Y. Bai, Ph.D. Thesis, NIKHEF and Utrecht University, 2007, [http://drupal.star.bnl.gov/STAR/files/Bai\\_Yuting.pdf](http://drupal.star.bnl.gov/STAR/files/Bai_Yuting.pdf) .
- [37] S. Afanasiev *et al.*, Phys. Rev. C **80**, 054907 (2009).
- [38] B.I. Abelev *et al.*, Phys. Rev. Lett. **99**, 112301 (2007).
- [39] A. Adare *et al.*, Phys. Rev. C **81**, 034911 (2010).
- [40] S. Afanasiev *et al.*, nucl-ex/0706.3034.
- [41] [http://rnc.lbl.gov/hft/docs/hft\\_final\\_submission\\_version.pdf](http://rnc.lbl.gov/hft/docs/hft_final_submission_version.pdf); S. Kleinfelder *et al.*, Nucl. Instr. Meth. A **565**, 132 (2006).
- [42] [http://drupal.star.bnl.gov/STAR/system/files/MTD\\_proposal\\_v14.pdf](http://drupal.star.bnl.gov/STAR/system/files/MTD_proposal_v14.pdf); Z. Xu, BNL LDRD project 07-007; L. Ruan *et al.*, J. Phys. G **36**, 095001 (2009); Y. Sun *et al.*, Nucl. Instr. Meth. A **593**, 307 (2008); Y. Wang *et al.*, Nucl. Instr. Meth. A **640**, 85 (2011).